J Mater Sci (2008) 43:270–280
DOI 10.1007/s10853-007-2171-z

In-situ observation of crack opening displacement (COD) in a metastable β titanium composite

Figen Kaya · Paul Bowen · Jun Liu

Received: 5 December 2006 / Accepted: 17 September 2007 / Published online: 17 October 2007

Abstract The interfacial strength of β-Ti composites was increased via ageing, to investigate the effects of interfacial strength on the crack opening. Prior to crack opening displacement (COD) measurements, the number and location of fractured fibres were identified by acoustic emission and fibre probing techniques. This was later used to model the crack opening for number of tests conditions, such as different values of applied stress intensity factor, interfacial strengths and test temperatures. COD measurements were performed on bridged cracks, which were obtained by cycling the specimens under tension–tension loading. Test results have shown that crack opening is affected by both intrinsic factors such as interfacial debonding and frictional sliding stresses and extrinsic factors such as the maximum applied stress intensity factor and test temperature.

Introduction

The fatigue crack growth resistance of silicon carbide fibre reinforced titanium matrix composites in the presence of an initial unbridged defect is affected by the initial maximum applied stress intensity factor, $K_{max,ini}$. As $K_{max,ini}$ increases, the fatigue crack growth resistance of a titanium matrix composite decreases. The eventual occurrence of crack arrest, or specimen failure is determined for a given test piece geometry by the number of fibres bridging the crack and the number of fibre broken in the crack wake, due to stress transfer from the cracked matrix [1]. Bridging of the fatigue crack occurs via debonding and sliding of high stiffness silicon carbide fibres primarily within the wake of the advancing crack tip. Hence, weak interfaces are often preferred as they promote debonding and sliding mechanisms. However, when weak interfaces are present, the transverse properties of the composites are often compromised and titanium metal matrix composites are often also subjected to such loading conditions [2].

Moreover, recent work [2–4] suggested that even the strongest interfaces debond ahead of the advancing matrix crack (as long as the bridging fibres have sufficient in-situ tensile strength to carry the increased stress transfer from the matrix) in titanium metal matrix composites. Furthermore elastic shielding is much more effective for composites containing stronger interfaces. In composite materials, fibres are in axial and radial compression due to their thermal expansion coefficient mismatch with the matrix. When a fatigue crack grows through the matrix it causes sliding between the fibre and matrix and as a result axial residual stresses are relieved, causing the fibre to elongate and the matrix to contract. This causes a residual crack opening displacement (CODr) that is believed to be proportional to the residual stresses and the slip distance [5].

The key parameters that affect crack opening have been established to be the debond (slip) length of the fibres which is proportional to crack opening displacement (COD) and the stress on the bridging fibres which is approximately independent of distance from the crack tip [6]. Thus, the fibres furthest from the crack tip may break

F. Kaya (✉)
Department of Metallurgical Engineering,
Faculty of Engineering,
Zonguldak Karaelmas University, Zonguldak, Turkey
e-mail: figenkaya81@hotmail.com

P. Bowen · J. Liu
School of Metallurgy and Materials and IRC in Materials Processing, The University of Birmingham, Birmingham B15 2TT, UK

because of the increased volume of fibre exposed to stress rather than because of the increased stress on the bridging fibres. However, the interactions between the maximum applied load value P_{max} and interfacial shear stress, τ, and COD are not well known. In this article, attempts are made to clarify these interactions using Ti β-21S composites of two different interfacial strengths (i.e. low interfacial strength in the as- received case and high interfacial strength as in the peak aged case). Crack opening displacements can be measured directly from loaded elektro-polished composite samples containing bridged fatigue crack, by in-situ SEM. In the meta-stable β titanium composites (Ti-β 21S/SCS-6) upon peak ageing, α precipitation causes a volume expansion in the matrix in regions close to the fibres and increases the modulus of the matrix. This causes increased compressive residual stresses, $\sigma_{res,}$ which in turn increase the interfacial strength of the composite. Indirect measurement of compressive residual stresses acting on the fibres could be carried out using the fibre push out tests as interfacial sliding stress,τ_{fr}, is a function of friction coefficient, μ and residual stress acting on the fibre/matrix interface, σ_{res}. It has been observed that both interfacial debonding and frictional sliding strength of Ti-β 21S/SCS-6 increase upon peak ageing [7]. Approximately 57% change was observed in debonding strength after peak ageing, where debonding stress of meta-stable Ti-β 21S/SCS-6 composite was increased from 75 to 118 MPa. Frictional sliding stress was also increased from 149 to 171 MPa [7].

Experimental work

The material used in this work was a β-21S/SCS-6 composite, which was produced by Textron (Lowell, USA) as 8-ply unidirectional lay-ups reinforced with a bulk fibre volume fraction of 37%. The composite was produced by the foil-fibre-foil hot pressing method. The specimens were cut into rectangular bars of dimensions $4 \times 2 \times 100$ mm^3. Peak ageing of composite specimens was carried out at a temperature of 540 °C for 8 h. Prior to the COD measurements, bridged fatigue cracks were obtained by cyclic loading of each specimen (with an initial notch size to width ratio, a_o/W of 0.24, initial notches were opened by using a diamond blade with a thickness of 150 μm), in tension–tension using a frequency of 10 Hz and an R (load ratio) of 0.5. For peak aged (PA) composite specimens both room temperature and 500 °C air tension–tension fatigue tests were conducted, while only room temperature tension–tension fatigue test was carried on as-received (AR) (solution treated) specimens. During the fatigue cycling the fibre failures were monitored using two PAC nano-30 acoustic sensors. For the specific set-up used for acoustic emission, all events having energy value higher than 100 μJ (arbitrary units) and amplitude value of 95 dB in combination were identified as fibre failure. These values were selected as fibre failure because acoustic sensors were calibrated using a pencil lead as a source of brittle fracture (simulating the brittle nature of SiC fibre fracture). Calibration of sensors were carried out while the specimen was loaded to 20 N and thus background noise sources such as hydrolic piston, loading jigs, etc. were also identified and later the background noise was filtered. Prior to in-situ COD measurements, probing of silicon carbide fibres was carried out in order to establish the number and the position of fractured fibres within the crack wake. Probing of individual fibres was carried out when the specimens were loaded in three-point bending under a maximum applied load of 30 N. This separates the fractured ends of any broken fibres and thus makes distinguishing fractured fibres easier. The probing itself was carried out by positioning a steel probe (which was attached to an X-Y-Z stage) to the carbon cores of each fibre with the aid of a long distance optical microscope**.** The resistances of each core along the fibres were measured [8]. Acoustic events were also monitored, in order to ensure that no further fibre fractures occurred during these probing procedures. Finally, in-situ tensile loading of pre-fatigued specimens was employed in order to measure the CODs of bridged crack, using a loading stage mounted in a FEG SEM. For in-situ SEM inspection, one side of the samples were polished before the samples were mounted. For crack opening displacement measurements, distinctive features (predominantly in the matrix and interface region) along the cracks were identified when the specimen were unloaded. After applied load was increased gradually, the opening of the cracks were monitored via displacement of the previously identified features. The crack opening displacement (COD) of the same specimens was also observed sequentially at 350 °C in vacuum, in order to assess the effect of decreased compressive residual stresses and matrix modulus on the crack (COD) profiles. A summary of tests carried out on the samples is given in Table 1.

Results and discussion

Fibre probing and acoustic emission

A typical fibre probing result is given in Fig. 1, showing the number and the locations of the fractured fibres within the bridged fatigue cracks. As can be seen from this schematic diagram, the bridging fibres fracture randomly within the crack wake due to variation in the fracture strength of the fibres. During tension–tension loading the fibre fractures were also recorded by acoustic emission and

Table 1 Summary of experiemental tests carried out on the samples

Heat Treatment	$K_{max,ini}$ values (MPam$^{1/2}$)	İnitial crack length used for predictions	Fatigue test temperature	In-situ test at room temperature	In-situ test at 350 °C	In-situ test applied load values (N)
As-received (AR)	27	Longer initial notch length used	Room temperature	Yes	Yes	400 and 880
Peak aged (PA)	21	Longer initial notch length used	Room temperature	Yes	Yes	700
Peak aged (PA)	19	Actual initial notch length used	Room temperature	Yes	Yes	866
Peak aged (PA)	19	Longer initial notch length used	500 °C in air	Yes	Yes	880

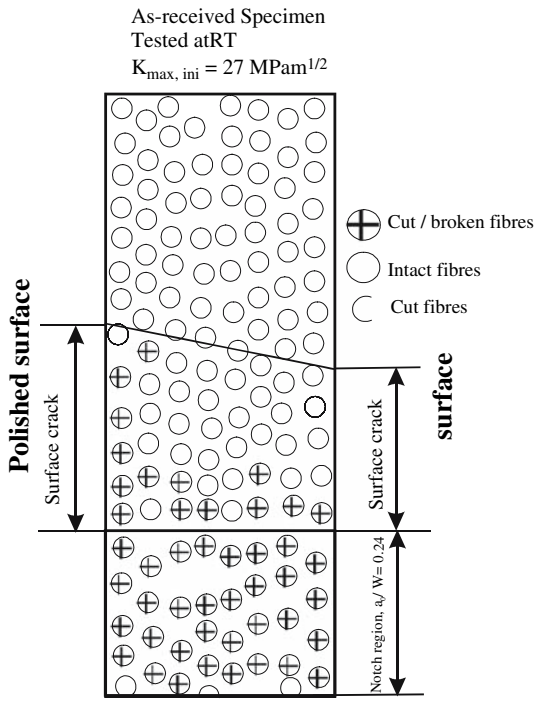

Fig. 1 A typical schematic diagram showing the fractured silicon carbide fibres within the crack wake of as-received composite, tested in tension–tension at $K_{max,ini}$ = 27 MPam$^{1/2}$ to crack arrest

a typical response of a composite specimen is given in Fig. 2. The fibre fractures are marked with arrows. A total of 11 fibre fractures were recorded during fatigue loading of this as-received specimen tested under $K_{max,ini}$ of 27 MPam$^{1/2}$, whereas 14 were detected by fibre probing (see Fig. 1). Both fibre probing and acoustic emission results have shown that higher number of fibres fracture when the composite was loaded to higher stress intensity factor values, as shown in Table 2. At room temperature the as-received (AR) specimen fatigued at $K_{max,ini}$ of

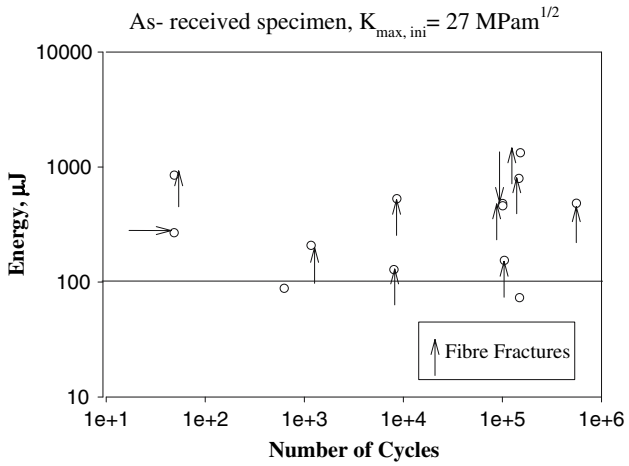

Fig. 2 Acoustic events that are identified as fibre fractures during the tension–tension fatigue test

Table 2 Number of fibre fractures detected during fatigue tests

Composite sample	$K_{max,ini}$ (MPam$^{1/2}$)	Fibre fracture detected	
		Fibre probing technique	Acoustic emission
AR	27	14	11
PA	21	10	6
PA	19	4	4
PA (500 °C, air)	19	30	12

27 MPam$^{1/2}$ exhibited the highest number of fibre fractures (11 fibre fractures were recorded by acoustic emission) as the maximum stress intensity factor value applied was the highest. However, when the specimen was tested at elevated temperature (500 °C) in air, the number of fractured fibres increased even though the maximum applied stress intensity factor value was 19 MPam$^{1/2}$, where 30 and 12 fibre fractures, were detected by fibre probing and acoustic emission, respectively (see Table 1). This suggests that the carbon coated silicon carbide fibres were more susceptible to fracture in an aggressive test environment (i.e. high temperatures with an air atmosphere). Information of how many fibres fractured and how they are located within the crack wake were later used during the prediction of crack opening profiles. For example, samples with high number fractured fibres located next to initial notch were treated as having longer initial unbridged defect size as explained in the next section.

In-situ observations

Figure 3a shows a typical fatigue crack of a composite occurred under tension–tension loading. This crack exhibits a residual crack opening displacement (CODr) in unloaded condition. In-situ observations of the composite revealed that crack opening displacement opens up further when an external applied load was applied, as shown in Fig. 3b.

The half crack opening displacements versus x positions, which represents the distance from the edge of the samples, of both as-received and peak aged composite specimens tested under a range of initial maximum applied stress intensity factor values, are plotted in Figs. 3–8. For a given applied load, the experimentally measured crack opening displacements along the fully bridged fatigue crack in the specimen are represented as dots. The predicted half crack opening and corresponding interfacial shear stress, τ, operating at the interface were numerically calculated by a FORTRAN programme using a model developed by Liu [9–11] and are represented by the continuous lines. According to the model developed by Liu, the half crack opening displacements, u(x) and bridging traction acting on the crack wake, $p(x)$ are a function of one another and the bridging tractions and COD profiles can be predicted simply from input data of specimen dimensions and known material parameters such as fibre volume fraction, Young's modulus and Poisson's ratio. Material parameters such as, the modulus of the matrix and fibre, Poisson's ratios of the fibre and matrix, fibre volume fraction, fibre radius used for the numerical calculations are listed in Table 3 [12–13]. Detailed information on the calculation method used is given in the appendix. The predicted half crack opening displacements without any fibre bridging, $p(x)$, are also shown in Figs. 3–7 as dashed lines. During the calculation of the crack opening, two different initial notch lengths are used for the specimens, with a number of broken fibres identified within crack wake located close to the tip of the initial notch by fibre probing. This may act in effect as an increased initial notch length and may change the geometrical factors of the specimen such as the "effective" a_o/W value. The predicted lines with code "a" represent calculated values using the actual initial notch length, whereas predicted lines with "a" represent the calculated half crack opening displacements using an increased notch length, depending on the number of fibre rows broken within the bridged fatigue crack. Similar treatments are conducted for all specimens having a number of broken fibres located close to the tip of the initial notch (except for the specimen tested at 19 MPam$^{1/2}$ which exhibited only four broken fibres in the crack wake).

In-situ observations revealed the existence of a residual crack opening displacement measured from the crack profiles when the specimens are unloaded, as shown in Fig. 3a. The residual crack opening displacements are related to axial compressive stresses on the fibre/matrix interfaces, which occur during the cooling of the composite due to differences in the thermal expansion coefficients of the fibre and the matrix [2]. Hence in order to make different crack profiles comparable, this residual crack opening displacement values are subtracted from the crack opening displacement values measured under various load values.

Room temperature in-situ tests

During in-situ observations, for similar crack lengths, the crack opening displacement (in this manuscript when the crack opening displacement is referred, half of the total opening of crack profile is meant for all samples) of the specimen under a higher applied load is observed to be greater than that of the specimen under a lower applied load as shown in Figs. 3–7.

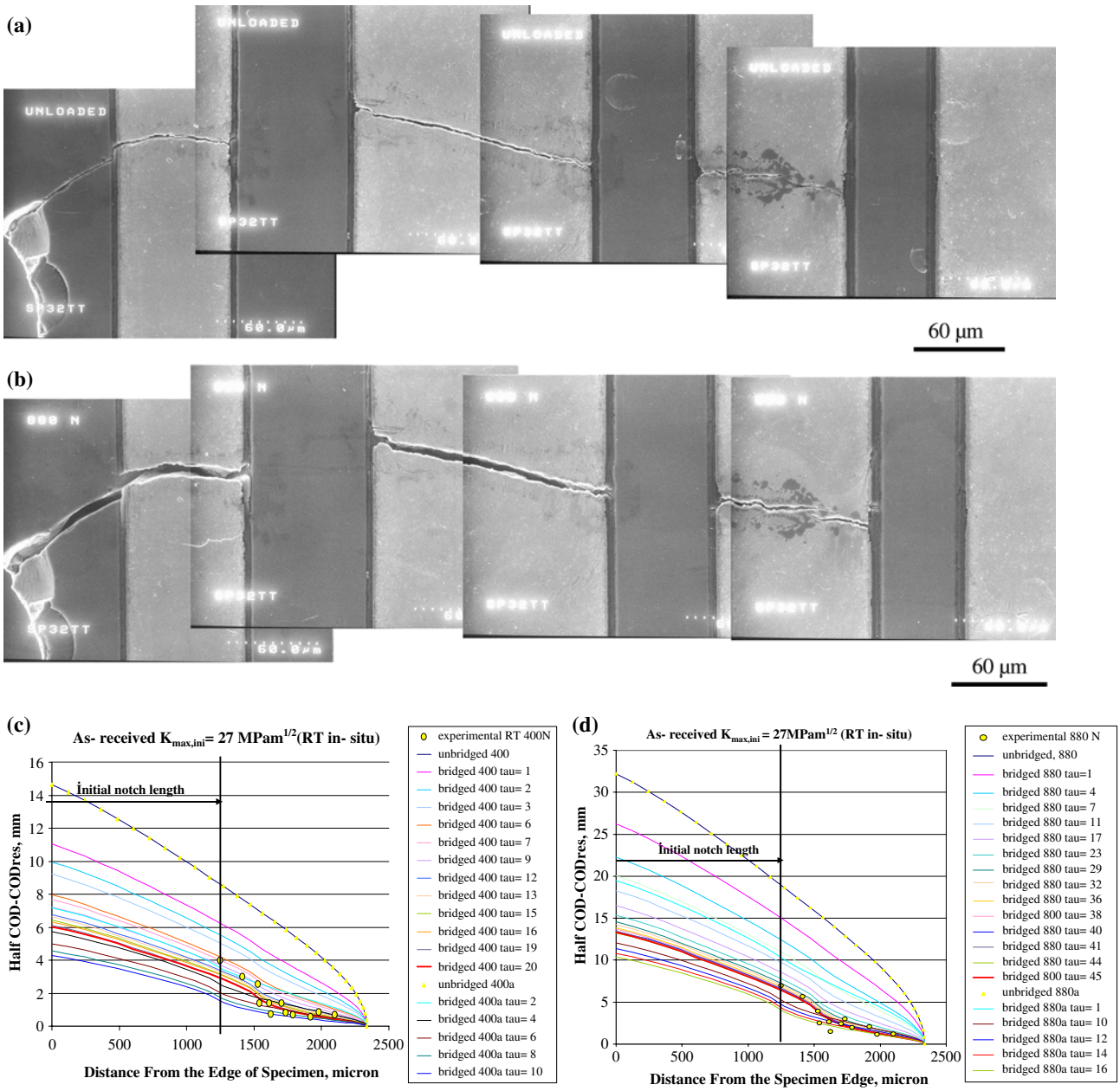

Fig. 3 (**a**) SEM micrographs showing a typical fatigue crack of a composite previously tested in tension–tension, (**b**) SEM micrograph showing a typical fatigue crack of a composite previously tested in tension–tension. Fatigue crack opens further upon loading, (**c**) Crack opening displacements of as-received specimen tested at initial maximum stress intensity factor value of 27 MPam$^{1/2}$ under 400 N, (**d**) Crack opening displacements of as-received specimen tested at initial maximum stress intensity factor value of 27 MPam$^{1/2}$ under 880 N

For all test conditions (both peak aged and as-received conditions at ambient and elevated temperature in-situ tests), the τ values which represent the compressive residual stresses on the interfaces required to achieve sufficient stress transfer from the matrix to the high strength fibres increase with increased maximum monotonic load P_{max}, applied for tension–tension in-situ loading. The results for a room temperature in-situ test of an AR specimen tested at a maximum initial stress intensity value of 27 MPam$^{1/2}$ are shown in Fig. 3c and d. The half crack opening displacements versus x positions, which represents the width of the specimen, has been plotted. The dots shown in Figs. 3–7 represent the experimentally measured crack opening displacements along the fully bridged fatigue crack of the specimen. The lines show (for a given applied monotonic load) the predicted half crack opening and corresponding interfacial shear stress, τ operating at the interface and have been numerically calculated using

Table 3 Materials parameters used for predicted crack opening displacement profiles, interfacial shear stress values, τ, and bridging traction values, $p(x)$ [11, 12]

Matrix modulus (Gpa)	75	Matrix volume fraction (%)	65
Fibre modulus (Gpa)	420	Fibre volume fraction (%)	35
Poisson's ratio of matrix	0.33	Fibre radius (μm)	70
Poisson's ratio of fibre	0.17		

the specimen geometry [9–11]. The crack opening displacements without any fibre bridging are also shown in Fig. 3c and d, as dotted lines. More detailed information on the prediction of crack opening displacements can be found elsewhere [9–11]. In total fourteen broken fibres were found within this AR specimen of which ten are located next to the notch tip, as can be seen from Fig. 1. Thus, the lines with 400a were plotted using an initial notch length of 1.227 mm, where the lines with 400 were plotted using an initial notch length of 1.527 mm, as explained above. The results have shown that the experimental values are in better agreement with the predicted half crack opening displacements calculated, using an initial notch length of 1.527 mm as shown in Fig. 3c and d. This shows that those broken fibres located next to the tip of the initial notch indeed have increased the effective initial notch size. The experimental values fall well below the dotted lines of the unbridged crack opening displacements as shown in Fig. 3c, indicating that fibre bridging is achieved in this particular specimen. The τ value of the best fit predicted opening to the experimentally measured crack opening displacements is found to be 20 MPa, which is much lower than experimentally measured interfacial shear strength value of 80 MPa for AR Ti-β 21S/SCS-6 composite, using fibre push out tests [7, 14]. It must be noted that the comparison of interfacial sliding stresses measured by fibre push out and predicted values using the fibre pressure model must be used in the context that in the fibre push out test the displacement of the fibre from the matrix is in the magnitude of 100 microns compared to displacement of the fibre within the crack wake which is in the magnitude of 10 microns. Therefore the values derived from the push out test and from the fibre bridging model should be used for relative comperison only. Figure 3d shows the half crack opening displacements for the same specimen under higher maximum applied monotonic load value of 880 N. As can be seen from Fig. 3c and d, the crack opening displacements increase with increased maximum applied load. The opening under 400 N is found to be 6 μm whereas the opening under 880 N is approximately 14 μm (here the crack opening displacement values at the edge of the specimens were used in order to simplify the reading the graphs). The shear stress at the interface, τ (here τ values were selected as the best fitted curve values, which is indicated with a thicker line), also increases with increased applied load, indicating that if external applied stress is higher the stress on the bridging fibres is also higher. In the AR condition, the τ value is found to be increasing from 20 to 45 MPa, which is still lower than that measured by fibre push-out, for applied load values of 400 and 880 N, respectively.

Figure 4 shows the half crack opening displacements for a PA specimen, which was cycled under maximum applied stress intensity value of 21 $MPam^{1/2}$ to crack arrest. Although, these AR and PA specimens were fatigued under different initial applied stress intensity values due to differences in their catastrophic failure/crack arrest transition values, their total crack lengths were broadly similar (thus the approximate volume fractions of fibres bridging the cracks were similar (24% for ~800 μm crack length and 25% for ~650 μm crack lengths for AR and PA conditions, respectively) enabled the crack opening displacements for a given maximum applied load value to be compared. Although maximum applied load value (700 N) was slightly lower than maximum external load value of 880 N applied to as-received specimen, half crack opening displacement was observed to be half of that observed in as-received specimen, as shown in Fig. 4. The best fit predicted interfacial shear stress value for the PA composite was higher than that for the AR composite under maximum applied load value of 700 N. The predicted shear stress for the AR composite was 45 MPa under 880 N whereas the τ value for the PA composite was predicted to be 51 MPa under a maximum applied load of 700 N. This confirmed the earlier assumption that the interfacial shear strength, τ, of the PA composite was higher than that of the AR composite. This was also confirmed by fibre push out tests [7, 14]. The results presented in Figs. 3a and 4 indicate that the stress transfer from the matrix to the high stiffness silicon carbide fibres was higher due to increased frictional sliding stresses acting on the interfaces which in turn may explain the reduced catastrophic failure/crack arrest transition of the PA composite (23–27 $MPam^{1/2}$) compared to that of AR composite (>34 $MPam^{1/2}$) [1].

Figure 5 shows the observations obtained from in-situ tests of a PA specimen which was initially fatigued under initial maximum applied stress intensity value of 19 $MPam^{1/2}$. As only four fractured fibres were identified by fibre probing, the original initial notch length was used for the predictions. The total crack length of this specimen was measured as ~650 μm, which was comparable to the total bridged crack length of the PA specimen tested at $K_{max,ini}$ = 21 $MPam^{1/2}$. Both crack opening and the τ values under 866 N were found to be smaller than that of the specimen tested at $K_{max,ini}$ = 21 $MPam^{1/2}$ under 700 N maximum applied load. CODs were ~6.5 μm and 39 MPa under 866 N and ~7.5 μm and 51 MPa under 700 N for

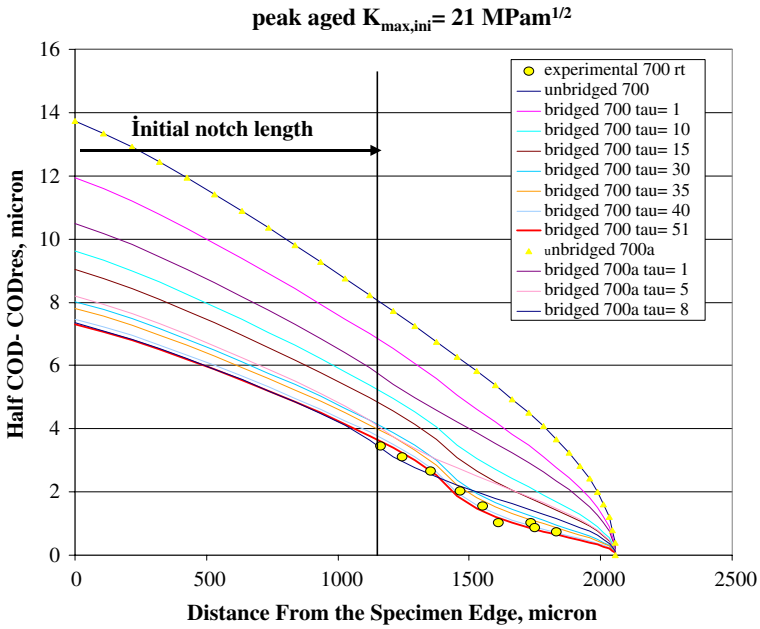

Fig. 4 Specific half crack opening displacements of peak aged specimen tested at initial maximum applied stress intensity factor value of 21 MPam$^{1/2}$

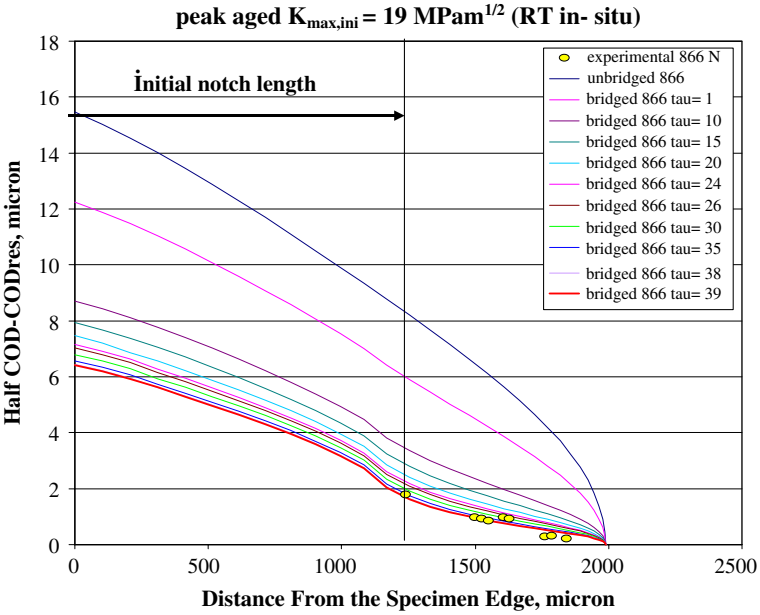

Fig. 5 Specific half crack opening displacements of peak aged specimen tested at initial maximum applied stress intensity factor value of 19 MPam$^{1/2}$

specimens tested at initial maximum applied stress intensity factor values of 19 and 21 MPam$^{1/2}$, respectively, as shown in Figs. 4 and 5. As both crack opening displacement, COD and interfacial shear stress, τ values were higher for a specimen which was initially cycled under higher $K_{max,ini}$ values than those of a specimen tested under lower $K_{max,ini}$ values, it may be concluded that both COD and τ were influenced by the maximum applied initial stress intensity factor values.

The half opening was found to increase when the specimen was tested at elevated temperature in air, prior to in-situ tests (see Fig. 6). This particular specimen which was tested under initial maximum stress intensity factor value of 19 MPam$^{1/2}$ exhibited many fibre fractures within the crack plane (see Table 1). Thus, the tension–tension fatigue test was terminated before the specimen failed in order to assess the effect of the fractured silicon carbide fibres on the crack opening displacements. The experimental results show that even though a large number of fibres fractured in the crack wake (total 30 fibres, 8 of them next to the polished surface of the specimen where the in-situ observations were carried out), fibre bridging still took place. However, the crack opening of this composite specimen was much larger than the opening observed in the

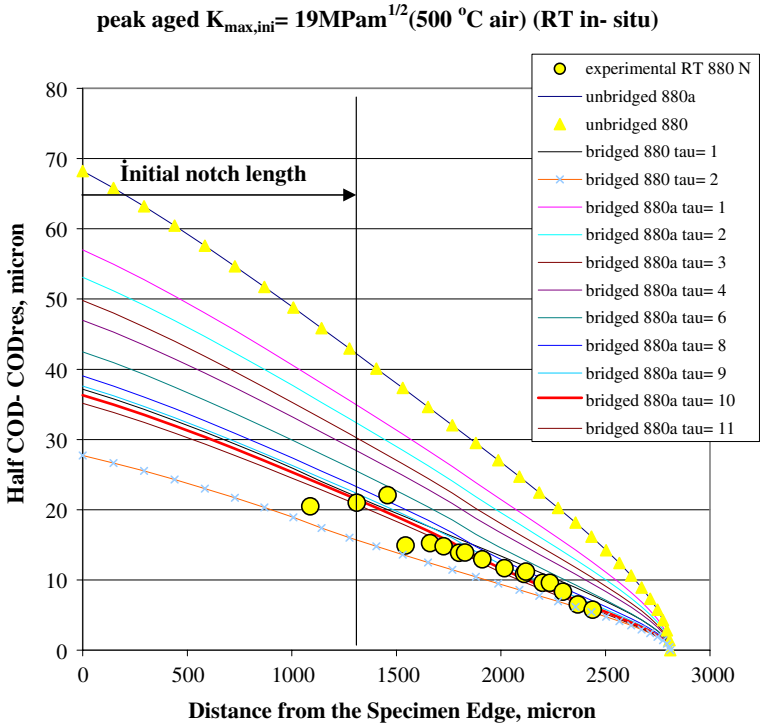

Fig. 6 Ambient temperature crack opening displacement of peak aged specimen which was fatigue tested under $K_{max,ini}$ = 19 MPam$^{1/2}$ at 500 °C in air

specimen tested under similar maximum initial stress intensity factor value of 19 MPam$^{1/2}$ at room temperature (Fig. 5).

The crack opening displacement of the specimen that was fatigue tested at 500 °C in air, was found to be 38 μm, where the crack opening of the specimen tested at room temperature was 6.5 μm, as shown in Figs. 5 and 6. In contrast to earlier results (which were observed for both PA and AR composites fatigued at room temperature) where the interfacial shear stress increases with increased crack opening displacements (see Figs. 3–5), the interfacial shear stress on the bridging fibres was found to be decreasing with increased CODs in this specimen. The interfacial strength (which was predicted to be 10 MPa, as shown in Fig. 6) was much lower than interfacial strength measured for Ti-β 21S/SCS-6 composite in PA condition (unfatigued specimens) by fibre push out tests [7, 14]. The mean strength of the fibre/matrix interface for the unfatigued PA composite was measured to be 137 MPa [11]. However, the interfacial strength values measured with fibre push out tests and the predicted interfacial sliding stresses should only be used for relative comparison for a given properties. Having said that similar trend of decreasing interfacial strength is also observed from fibre push out test on a specimen that was prefatigued at 500 °C in air [7, 14]. Where interfacial strength values as low as 22 MPa were measured that could be compared to interfacial slidind stress value of 10 MPa predicted using the fibre bridging model.

The fibre push out results indicated that the strength of fibre/matrix interfaces degrade considerably within the fatigue crack wake. The mean strength of interfaces measured within the crack wake was 21 MPa (interfacial strength values vary within the crack wake therefore a group of fibres were tested and the mean strength was calculated. Minimum strength value measured was 15 MPa), whereas the mean strength was measured to be 87 MPa (minimum was 30 MPa) within the region further away from the crack wake. Larsen [15] also measured very low interfacial strength values ranging from 9 to 1 MPa in a composite slice taken from within the fatigue crack plane of specimen tested in air at 650 °C. The oxidation of the carbon coating of the ceramic fibres is believed to be the key issue for the degradation process.

The elevated temperature in-situ tests

The half crack opening displacements of a specimen, which was tested in-situ at 350 °C was observed to increase from ~6 to ~8 μm with increasing test temperature, as shown in Figs. 3c and 7. At an applied load of 400 N the interfacial shear stress, τ value of 7 MPa for the as-received specimen tested at 350 °C in vacuum was found to be lower than the interfacial shear stress value of 20 MPa predicted for the same crack profile at room temperature, as shown in Figs. 3c and 7. Experimental results combined with existing models have shown that the interfacial shear

stresses on the bridging fibres were decreasing for this particular specimen even though the crack opening displacement was found to be increasing compared to room temperature observations. This contradicts the earlier result, where the interfacial shear stresses increases with an increased half crack opening displacement (as the maximum applied load value increases) as shown in Figs. 3c and d. This drop in the interfacial shear stress value was believed to be caused by the diminished residual stresses due to increased testing temperature. The thermal coefficient of linear expansion (CTE) of meta-stable β-21S titanium (beta annealed plus peak aged at 540 °C for 8 h) increases from 7.2 to 8.8 (10^{-6}/°C), when the testing temperature is raised from 25 to 300 °C [16]. The thermal linear expansion coefficient of the SCS-6 fibre also increases from 2 to 2.5 (10^{-6}/°C) [13]. Therefore the magnitude of the compressive residual stresses operating at the interfaces decreases. The radial compressive residual stresses on the fibres are often related to interfacial bonding and sliding stresses as this compression ensures the fibre and the matrix are kept in close contact [17]. However, the observations in this work were made on the fully bridged crack region, fibre/matrix interfaces are already debonded (as a minimum within the fibre/matrix sliding distance), but interfacial frictional sliding stresses were still operating at the debonded interfaces. Hence, any change in the magnitude of the compressive residual stresses due to change in the thermal linear expansion coefficients of the fibre matrix will be related to interfacial frictional sliding stresses.

Figure 8 shows crack opening displacements for PA specimens, which was previously tested at maximum initial stress intensity factor value of 19 MPam$^{1/2}$. The crack opening displacements of this particular specimen were observed to increase with increased testing temperature. The half opening of best fit predicted curve was about 6 μm at room temperature whereas it was measured about 8 μm at 350 °C, as shown in Figs. 5 and 8. This increase in the opening was believed to be caused both by the decreased stiffness of the PA Ti-β 21S matrix and decreased compressive radial residual stresses. The interfacial shear stress was also found to be decreasing with the increased test temperature in the PA condition. The interfacial shear stress, τ value of the best fit predicted crack opening was calculated to be 39 MPa at ambient temperature whereas τ was predicted to be 17 MPa when tested at 350 °C. Hence, the stresses transferred from the titanium matrix to ceramic fibres are deduced to be decreased in the PA condition when the composite was tested at elevated temperatures.

Conclusion

Crack opening displacements of meta-stable β titanium metal matrix composites with different interfacial strengths were investigated. It was found that the opening of a fully bridged crack increases with increasing maximum applied stress values. The interfacial shear stress was also found to increase with increased applied stress

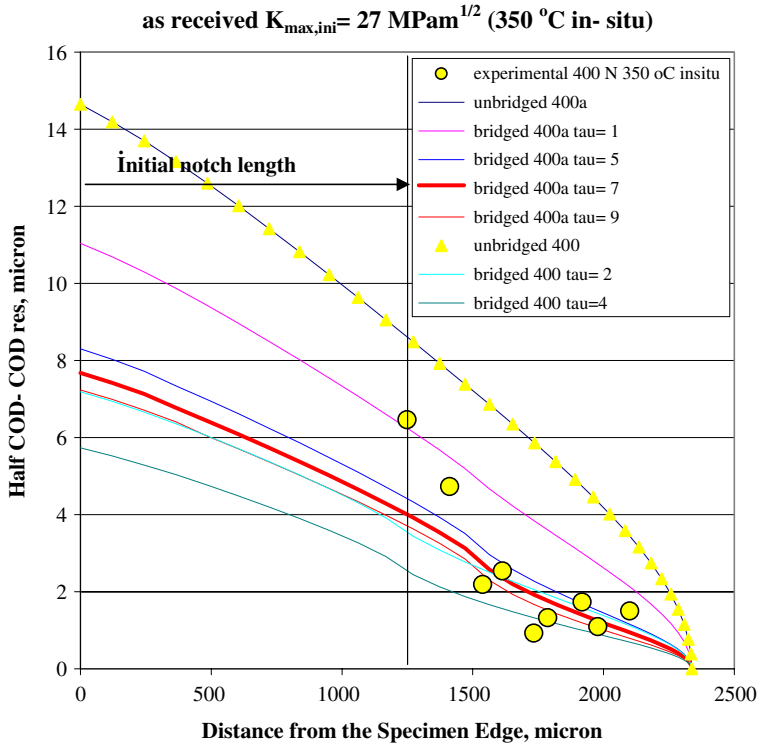

Fig. 7 Crack opening displacement of as-received composite at 350 °C, vacuum (Prior to tension–tension in-situ test the specimen was cycled under $K_{max,ini}$ = 27 MPam$^{1/2}$ in air)

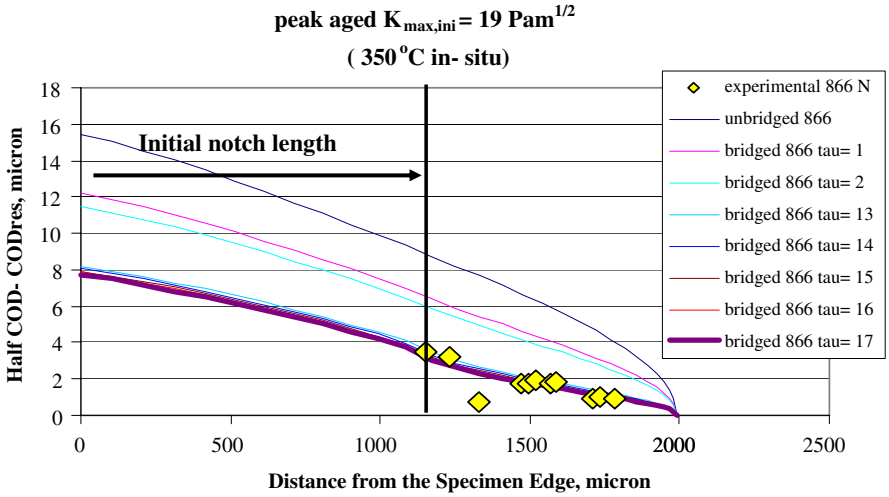

Fig. 8 In-situ crack opening displacement of peak aged specimen at 350 °C, vacuum (specimen was initially fatigued at initial maximum applied stress intensity factor value of 19 $MPam^{1/2}$)

at a given temperature, indicating that if the external stress on the composite was higher the stress transferred from matrix to the bridging fibres was also higher.

Both crack opening and interfacial shear stress appeared to be influenced by the maximum applied stress intensity factor values. Crack opening and interfacial shear stress on the bridging fibres in a peak aged specimen which was fatigued at higher initial stress intensity factors was predicted to be larger than those of a specimen tested at lower stress intensity factors.

Crack opening displacement of PA specimens was found to be lower than that of AR specimens. It is believed that increased interfacial frictional sliding strength due to increased compressive residual stresses may play a role.

The crack opening displacement of both AR and PA composites was increasing, while the predicted interfacial shear stresses were found to be decreasing with increased in-situ test temperature. It was deduced that reduced radial compressive residual stresses due to decreases in the CTE of the fibre and matrix played an important role. The results also show that the relation between interfacial shear strength and crack opening displacement is complex and further examination is necessary in order to understand fully the interaction of these parameters and this is the subject of our current research.

Appendix (Prediction of stresses in bridging fibres)

The stresses in bridging fibres are assumed to be $p(x)/V_f$, where $p(x)$ is the bridging traction to be solved, and V_f is the fibre volume fraction. The governing equations used to predict $p(x)$ are:

$$u(x)=\frac{4}{E'}\int_x^a\left\{\int_0^{a'}G(x',a',W)[\sigma_a(x)-p(x')]\mathrm{d}x'\right\}G(x,a',W)\mathrm{d}a' \tag{A1}$$

$$p(x)=\frac{E_f V_f \sigma_a}{2E_c}\left\{\sqrt{1+\frac{16E_c^2E_fV^2u(x)\tau}{E_c^2V_f^2\sigma_a^2\rho}}+1\right\} \tag{A2}$$

$$\int_{a_0}^{a}p(x)\mathrm{d}x=\frac{1}{k}\int_{a_0}^{a}c(x)\mathrm{d}x \tag{A3}$$

where $u(x)$ is the half crack opening displacement (COD) profile, E_f and E_c are the elastic moduli of the fibre and the composite, respectively, σ_a is the applied stress on the composite, τ is the interfacial sliding stress, ρ is the fibre radius, $G(x, a, W)$ is a weight function, E' is the modulus of an orthotropic material containing a plane stress crack normal to the loading direction, k is a constant for a given specimen width, and $c(x)$ is the bridging traction following the fibre pressure models [17–19]. Expressions of $G(x, a, W)$ and E' are available elsewhere [18].

Equation A1 comes from continuum mechanics, and has been widely employed in shear-lag models. Equation A2 is similar to that derived by Danchaivijit and Shetty [20]. However, a difference is that, instead of being treated as a constant [20], τ in the present paper is considered to be a variable (because of the Poisson ratio effect), and is expressed as,

$$\tau(x) = \tau_0\{1 - [B1p(x) + B2\sigma_a]\} \quad \text{(A4)}$$

where,

$$B1 = \frac{\mu E_m}{2D\tau_0 E_f} \upsilon_f \frac{1}{V_f} \quad \text{(A5)}$$

$$B2 = \frac{\mu E_m}{2D\tau_0 E_0} (\upsilon_f - \upsilon_m) \quad \text{(A6)}$$

and where τ_0 is a constant shear stress (similar to that used elsewhere [20] when the Poisson ratio effect is neglected), μ is the friction coefficient, v is Poisson's ratio, and E_m is the elastic modulus of the matrix. The derivation of Eqs. A4–A6 follows the procedure given elsewhere [21], but the expressions are slightly different. Note that Eq. A2 applies to both the steadystate and non-steady-state regions of the crack [20], and hence is more general than equations such as

$$p(x) = 2V_f \sqrt{\frac{E_c E_f \tau_0 u(x)}{E_m(1 - V_f)\rho}} \quad \text{(A7)}$$

which was developed by Marshall, Cox, and Evans [22]. Indeed, Eq. A7 is a specific case of Eq. A1 when $p(x) > rlessS_a$, which implies steady-state crack growth. Equation A3 is an empirical relationship between the *average* bridging tractions obtained from Eq. A2 and those obtained from the fibre pressure model [17]. Based on independent in-situ SEM measurements of COD profiles along bridged cracks [8] and modelling using Eqs. A1 and A2, k is determined to be 1.06 and 1.0 for specimens with a width of $\sim$4 and $\sim$10 mm, respectively. Since the fibre pressure model [17] neglects the details of load transfer along the fibre–matrix interface, and is purely based on load balance, $c(x)$ can be easily calculated for a given specimen geometry under a given applied stress. Therefore, Eq. A3 can be used as a criterion to determine t_0, i.e., different assumed values of τ_0 are tested until the value of $p(x)$ satisfies Eq. A3. By using Eqs. A1–A6, the bridging tractions and COD profiles can be predicted simply from input data of specimen dimensions and known material parameters such as fibre volume fraction, Young's modulus and Poisson's ratio. The value of interfacial shear stress, although needed during the calculation, is not needed to be known a priori.

References

1. Kaya F, Liu J, Fox KM, Bowen P (1999) In: Wu XR, Wang ZG (eds) Fatigue' 99, Proceedings of the 7th international fatigue congress, Beijing, 1999, p 1429
2. Warrier SG, Majumdar BS (1997) Mater Sci Eng A237:256
3. Warrier SG, Majumdar BS, Miracle DB (1997) Acta Mater 45:4969
4. Warrier SG, Majumdar BS (1999) Metall Mater Trans A 30:277
5. Davidson DL (1992) Metall Trans 23A:865
6. Majumdar BS (1998) In: Mall S, Nicholas T (eds) Titanium matrix composites, mechanical behaviour. Technomic Publication, Pennsylvania, p 118
7. Kaya F, Bowen P (in press) Mater Sci Eng A, doi: 10.1016/j.msea.2007.04.096
8. Barney C (1995) PhD Thesis. The University of Birmingham, UK
9. Liu J (1999) PhD Thesis. The University of Birmingham, UK
10. Liu J, Bowen P (2002) Acta Mater 50:4205
11. Liu J, Bowen P (2001) Metall Mater Trans A34:1193
12. Fanning JC (1993) In: Eylon D, Boyer RR (eds) Ti metal21S property data. beta alloys in the 1990s. The Minerals, Metals and Materials Society, p 397
13. Bunsell AR, (1999) In: Bunsell AR, Berge MH (eds) Fine ceramic fibres. Marcel Deccer Inc., p 1
14. Kaya F (2003) PhD Thesis. The University of Birmingham, UK
15. Larsen E (1995) In: Blenkinshop PA, Evans WJ, Flower HM (eds) Titanium'95 science and technology. Proceedings of the 8th world conference on titanium, vol III. Birmingham, UK. 22–26 October 1995, p 2803
16. Materials Properties Handbook (1994) Titanium alloys. ASM International, p 58
17. Covey SJ, Lerch BA, Jayaraman N (1995) Mater Sci Eng A200:68
18. Ghosn LJ, Kantzos P, Telesman J (1992) Int J Fract 54:345
19. Cox BN, Marshall DB (1991) Fatigue Fract Eng Mater Struct 14:857
20. Danchaivijit S, Shetty DK (1993) J Am Ceram Soc 76(10):2497
21. Fox KM (1994) PhD Thesis. The University of Birmingham, UK
22. Marshall DB, Cox BN, Evans AG (1985) Acta Metall 33(11):2013